Research Article

Kun Ge, Dan Guo, Ben Niu, Zhiyang Xu, Jun Ruan and Tianrui Zhai*

Pump-controlled RGB single-mode polymer lasers based on a hybrid 2D–3D μ-cavity for temperature sensing

https://doi.org/10.1515/nanoph-2021-0462
Received August 19, 2021; accepted October 18, 2021;
published online October 29, 2021

Abstract: Single mode lasers, particularly red-green-blue (RGB) colors, have attracted wide attention due to their potential applications in the photonic field. Here, we realize the RGB single mode lasing in a hybrid two-dimension and three-dimension (2D–3D) hybrid microcavity (μ-cavity) with a low threshold. The hybrid 2D–3D μ-cavity consists of a polymer fiber and a microsphere. Typical RGB polymer film consisting gain materials are cladded on a fiber. To achieve single mode lasing, the polymer fiber therein serves as an excellent gain cavity to provide multiple lasing modes while the microsphere acts as a loss channel to suppress most of the lasing modes. Mode switching can be realized by adjusting the pump position. It can be attributed to the change of coupled efficiency between gain μ-cavity and loss μ-cavity. Our work will provide a platform for the rational design of nanophotonic devices and on-chip communication.

Keywords: 2D–3D μ-cavity; mode switching; polymer fiber; RGB; single mode laser.

1 Introduction

The whispering gallery mode (WGM) microcavity (μ-cavity) lasing with small mode volume and high quality (*Q*) factor has attracted a lot of attention due to the novel physical properties and potential applications [1–5], such as biochemical and biological sensing [6–10], aerostatic pressure sensing [11, 12], white light sources [13–15] as well as full color displays [16–18]. Moreover, the single-mode WGM lasing is vital for various photonic applications and anti-counterfeiting. Generally, the single mode lasing can be achieved by reducing the size of the resonator cavity so that the free spectral range (FSR) exceeds the photoluminescence (PL) emission range of the gain materials until only one lasing mode exists in the cavity [19–21]. Another method for single mode lasing is utilizing the distributed feedback grating [22–24]. The coupled μ-cavity based on the Vernier effect [25–27] and the parity-time symmetry breaking [28–30] have been reported to achieve the single-mode lasing. The fiber-based lasers [31–33] have been attracted much attention owing to the laser is simple preparation. In the past years, the WGM μ-cavity have been fabricated in various shapes, such as microrings [34], microtubes, microrods [35–37], micropolymer bottle [38, 39] and so on.

Single mode laser, can be achieved by a coupled cavity in which one μ-cavity serves as gain cavity to provide multiple lasing resonant modes, and the other μ-cavity can act as a loss channel to suppress most of the lasing modes. The red-green-blue (RGB) single mode lasing can be obtained by altering the organic polymer gain materials in coupled μ-cavity. Moreover, the tunable lasing has hold great attention. Generally, the tunable lasing can be achieved by altering the effective refractive index and temperature [40, 41].

However, these strategies usually hinder the popularization of single-mode lasing owing to requiring precise manipulation and complicated fabrication. Here, we demon-strate a simple and general approach to realize tunable RGB single mode lasing with a low threshold in hybrid two-dimension and three-dimension (2D–3D) μ-cavity. The polymer fiber serves as a 2D μ-cavity and the polystyrene microsphere (PSP) can act as a 3D μ-cavity in hybrid μ-cavity. The 2D μ-cavity is isotropic and 3D μ-cavity is tunable and flexible. To achieve single mode lasing, the polymer fiber therein serves as an excellent gain μ-cavity to provide multiple lasing modes while the PSP acts as a loss channel to suppress most of the lasing modes. The hybrid 2D–3D coupled μ-cavity enable single

***Corresponding author: Tianrui Zhai,** College of Physics and Optoelectronics, Faculty of Science, Beijing University of Technology, Beijing 100124, China, E-mail: trzhai@bjut.edu.cn. https://orcid.org/0000-0003-1922-2386
Kun Ge, Dan Guo, Ben Niu, Zhiyang Xu and Jun Ruan, College of Physics and Optoelectronics, Faculty of Science, Beijing University of Technology, Beijing 100124, China

mode lasing when all but one of the lasing modes is suppressed.

There are two main strategies to achieve the RGB laser. The RGB laser can be obtained by mixing three different gain materials, which is higher integration. And the lasing cannot be tuned alone and the cascading effect may have effect on the lasing mode. However, parallel the three trichromatic lasers are an effective way to realize the RGB laser. This strategy can adjust the RGB laser one by one. And it will be potential applications in light sources, anti-counterfeiting and full color display. This RGB lasers can be tuned wide range for International Commission on Illumination (CIE) 1931 color. Therefore, we adopt the parallel strategy to obtaining the RGB laser in the experiment.

The RGB single mode laser can be designed easily by changing the types of the gain materials in the hybrid μ-cavity. So, we can achieve dynamic regulation of RGB single mode lasing in hybrid 2D–3D μ-cavity. Furthermore, the wavelength switch of single mode laser can be realized by adjusting the resonant modes owing to the different coupled efficiency between gain μ-cavity and loss μ-cavity. The numerically simulated electric field distributions includes two relational μ-cavity, the result indicates the mode selection mechanism in the coupled resonators. This work not only do we study the operating range of single mode, but also discuss the working range of multimode in hybrid μ-cavity. The RGB laser can have high transmission bandwidth, which may provide the rational design of nanophotonic devices and on-chip communication [42].

2 Fabrication of the RGB WGM laser

Three typical light-emitting molecules Rhodamine B (RhB, Tianjin Fuchen Chemical Reagents Factory, Tianjin, China), Fluorescein sodium salt (uranin A46092 AI LAN (Shanghai) Chemical Technology Co., Ltd, Shanghai, China) and disodium 4,4′-bis(2-sulfonatostyryl)biphenyl (S420 D-36543 Tianjin Heowns Biochem LLC, Tianjin, China) are used in this work. The blue-emitting material (S420) is dissolved in deionized water with concentration of 10 mg/ml, and the green-emitting material (uranin) and red-emitting material (RhB) are dissolved in ethanol with concentration of 9 mg/ml and 6 mg/ml, respectively. The polyvinyl alcohol (PVA) (S27039-500g, Beijing Honghu United Chemical Products Co., Ltd., Yuanye, Beijing, China) is dissolved in deionized water with the concentration of 16 wt%. The PVA solution serves as the matrix and adhesion agent. Then they are mixed with the volume ratio (1:1) under magnetic stirring for 30 min.

The frame consists of the fiber and PSP, which are commercial and do not need further treatment. The fiber diameter is 125 μm, and its effective refractive index is 1.45. The dye layer's thickness is about 30 μm, and the effective refractive index of microcavity is 1.55. The single mode lasing design principle and the fabrication progress are demonstrated in Figure 1a. The polymer fiber is fabricated by drop-coating (Supplementary Figure 1). There are the normalized absorption and PL (Supplementary Figure 2), respectively.

In the design of RGB single mode lasers based on the hybrid 2D–3D μ-cavity. The mode selection system is illustrated in the couple μ-cavity (in Figure 1a). The electric field intensity distribution in the transverse cross-section is numerically simulated by the commercial software COMSOL multi-physics 5.4. The results show that the mode selection mechanism in the coupled resonators (in Figure 1b). The polymer fiber can serve as a WGM μ-cavity to support multiple lasing modes within its gain band while the PSP can act as a loss channel to suppress most of the lasing modes in the coupled system. Both the polymer fibers and PSP show negligible deformation in the coupled μ-cavity. The optical bright field (left) and dark field (right) shows the same diameter of polymer fiber with different diameter of PSP in a coupled μ-cavities (in Figure 1c).

3 Spectra characterization of the RGB lasing

The PL emission spectra of RGB lasing are demonstrated when pumped by a nanosecond laser with wavelength of 343 nm (third harmonics from a 1030 nm Yb:YAG laser, repetition frequency of 200 Hz, and pulse width of 1 ns). Each of the polymer fiber μ-cavity is smooth and uniform, which helps to reduce the loss and threshold. It can be used as a high quality WGM μ-cavity to support optical feedback and oscillations.

As shown in Figure 2a–c, the PL emission spectra are under different pump power from 4.5 $\mu J/cm^2$ to 189.0 $\mu J/cm^2$, 7.6 $\mu J/cm^2$ to 189.0 $\mu J/cm^2$ and 2.3 $\mu J/cm^2$ to 45.8 $\mu J/cm^2$ with excitation on the blue-emitting, green-emitting and red-emitting gain materials, respectively. More details can be observed in the enlarged spectrum (top right illustration in Figure 2a–c). The bottom left illustration is the optical photos with different excitation power (light and dark field in Figure 2a–c). The PL images of the polymer fiber are captured by an optical microscopy, exhibiting bright ring-shaped patterns at the boundary and confirming the WGM resonance.

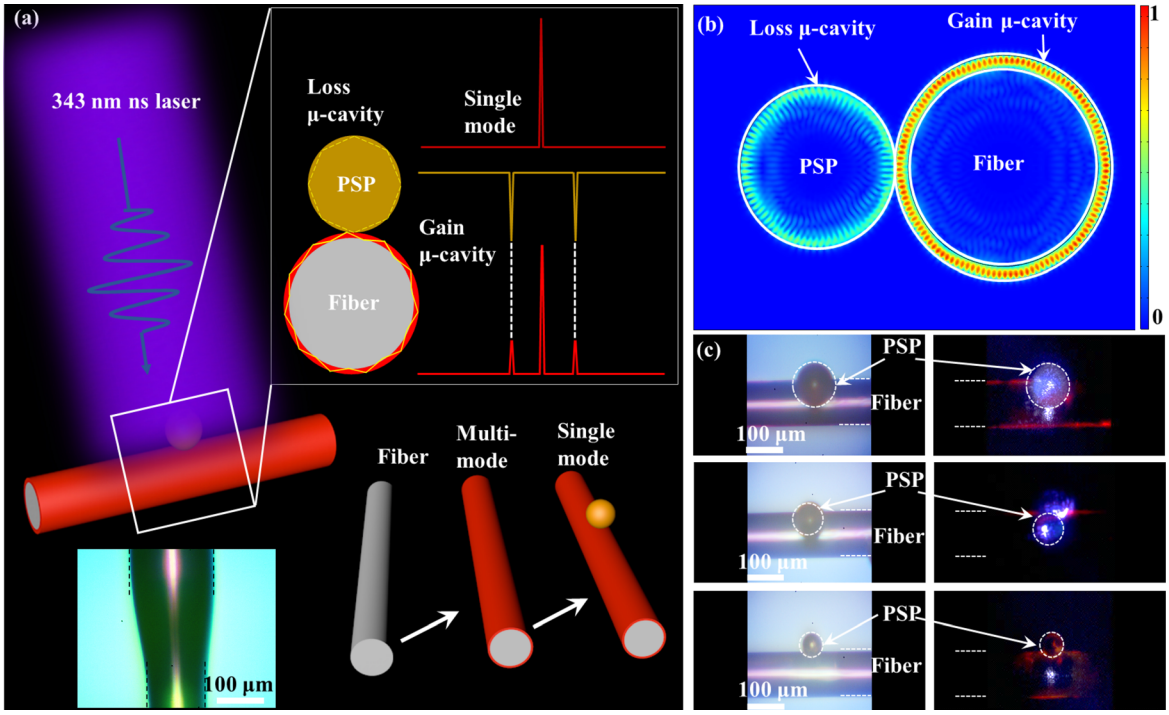

Figure 1: Mechanism of mode selection in the coupled μ-cavity.
(a) A schematic illustration of the fabrication progress and mode selection in hybrid 2D–3D μ-cavity. (b) Numerically simulated electric field distribution of the modes in the coupled system, indicating the mode selection mechanism in the coupled resonators. (c) The optical images of bright field (left) and dark field (right) and the same diameter of polymer fiber with different diameters of PSP.

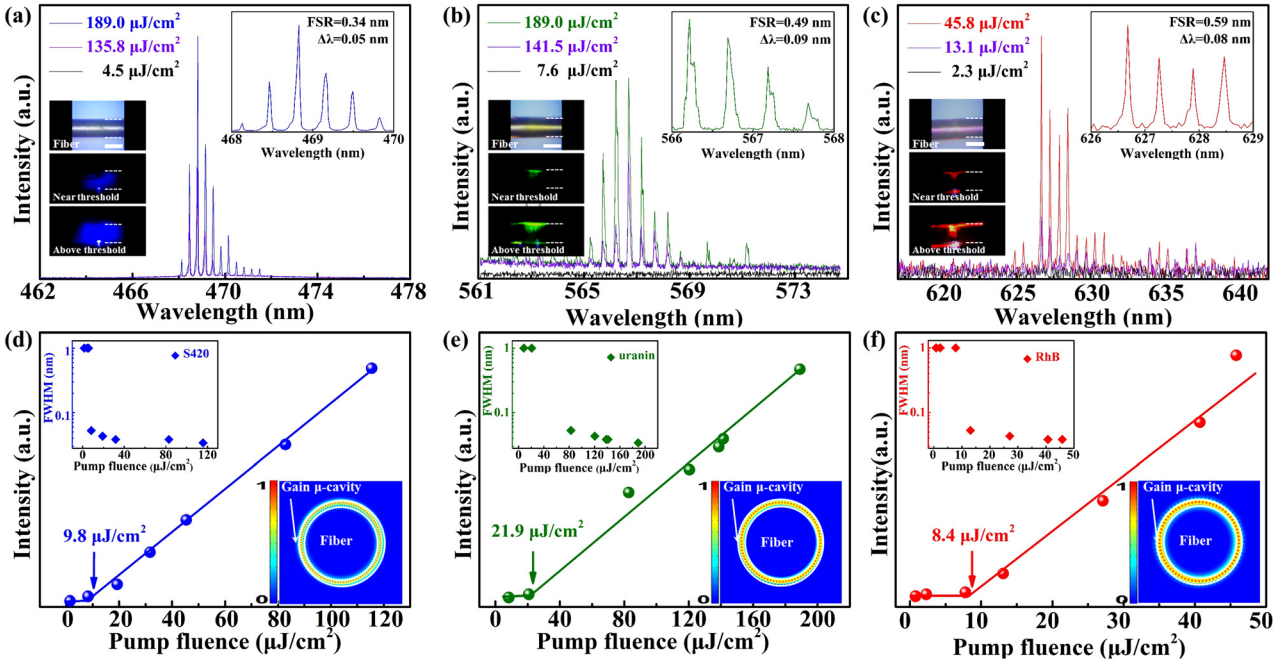

Figure 2: The RGB WGM lasing spectra.
(a–c) The spectra of WGM lasing with the excitation on the blue-emitting, green-emitting and red-emitting cavity. Bottom left illustration is the optical pictures under different pump power (light and dark field). Top right is the enlarged spectrum, respectively. Scale bars: 100 μm. (d–f) The relationship between pump power density and output intensity, the threshold are 9.8 μJ/cm², 21.9 μJ/cm² and 8.4 μJ/cm² marked by an arrow, respectively. Bottom right illustration is the simulated electric field intensity in transverse cross-section. Top left illustration is the FWHM at different pump fluence, respectively.

The relationship between pump power and output density are shown in Figure 2d–f. The threshold for the blue-emitting, green-emitting and red-emitting are 9.8 μJ/cm^2, 21.9 μJ/cm^2 and 8.4 μJ/cm^2 marked by arrows in Figure 2d–f, respectively. The low threshold indicates that the optical loss is small in the polymer fiber μ-cavity. Top left inset illustrates the relationship between the full width at half maximum (FWHM) and pump intensity for the WGM lasing (in Figure 2d–f). The bottom right illustration is the numerically simulated electric field distribution of the lasing mode in the isolated polymer fiber (Supplementary Figure 3). The higher order radial modes can be excited in the cavity (Supplementary Figure 4). The polymer fiber can act as a WGM resonance μ-cavity to support the stimulated radiation amplification and obtain multiple lasing modes. The refractive index of polymer is calculated and fitted by the spectroscopic ellipsometer (ESNano, ELLiTOP Sclentiflo Co., Ltd.).

The FSR and quality (Q) factor can be tuned by changing the polymer fiber diameter. As shown in Figure 3a, the mode spacing gradually increases with decreasing the μ-cavity diameter. The PL emission spectrum is modulated in three polymer fibers with different diameters above the threshold (in Figure 3a). The illustration shows the FSR are 0.36 nm, 0.61 nm, and 0.98 nm for the μ-cavity diameters of 228 μm, 134 μm, and 83 μm, and the line-widths ($\Delta\lambda$) are 0.12 nm, 0.19 nm, and 0.27 nm recorded by a spectrometer with resolution of 0.001 nm (the top right in Figure 3a), respectively. Further investigation of the FSR shows that an inversely proportional relationship exists between the mode spacing and the diameter, according to WGM resonance equation

$$m\lambda_m = \pi n_{eff} D \tag{1}$$

where λ_m is the peak wavelength, m is the mode number, n_{eff} is the effective refractive index, and D is the polymer fiber diameter, respectively. The theoretical calculation demonstrates the peak wavelength belong to first order transverse magnetic (TM) and transverse electric (TE) modes, and the corresponding mode number is from 1035 to 1042. The blue triangles represent peak wavelength of TE modes and the red squares represent peak wavelength of TM modes. In our experiment, the Q factor can be estimated over 5000 by using equation $Q = \lambda/\Delta\lambda$, where λ is 630 nm and $\Delta\lambda$ is 0.12 nm, indicating the μ-cavity has low optical loss. Moreover, the Q factor can be higher to 19,000 when the μ-cavity is smooth (Supplementary Figure 6). The peak wavelength can be well-fitted as shown in Figure 3b.

To obtain more information about the lasing characteristics, the size related measurements of the isolated polymer fibers are carried out. Hence, according to the WGM theory

$$\mathrm{FSR} = \frac{\lambda^2}{\pi D n_{eff}} \tag{2}$$

where λ is the peak wavelength. The relationship between FSR and the D are shown in Figure 3c. The dashed line is fitted with Eq. (2). The slope α is constant. Moreover, the calculation of Q factor is in the range from 2000 to 6000. The red squares indicate the relationship between Q factor and various diameters in the experiment (in Figure 3d). The spontaneous emission range of the isolated polymer fiber comes from the gain-doped and the highlighted area indicates lasing region as shown in Figure 3e.

To achieve single mode lasing, the polymer fiber therein serves as an excellent gain cavity to provide multiple lasing modes while the PSP acts as a loss channel to suppress most of the lasing modes in the 2D–3D hybrid μ-cavity. The single mode lasing with wavelength (λ = 626.15 nm) is indicated (in Figure 4a) under different pump fluence increasing from 45.4 μJ/cm^2 to 175.3 μJ/cm^2. The results demonstrate that the filtering effect is an effective way to realize single mode lasing due to the mode selection mechanism (Supplementary Figure 7). Moreover, the colors of the RGB single mode lasers can be designed easily by changing the gain materials. Figure 4e provides the normalized single mode lasing emission spectra and corresponding PL images. Therefore, we can achieve the single mode lasing in the coupled μ-cavity. Furthermore, the wavelength switch of single mode laser can be realized by adjusting the resonant modes owing to the different coupled efficiency between gain μ-cavity and loss μ-cavity (in Figure 4d).

According to the filtering effect, the polymer fiber therein serves as an excellent gain μ-cavity to provide multiple lasing modes while the PSP acts as the loss channel to suppress most of the lasing modes in the hybrid 2D–3D μ-cavity which enable single mode lasing when all but one of the lasing modes are suppressed by the loss μ-cavity. There are not bonding and anti-bonding modes in our configuration. The output lasing is controlled by the active cavity, and the passive cavity is mainly used as a filter in 2D–3D hybrid μ-cavity.

The laser mode will change owing to the different coupled efficiency in the coupled μ-cavity (Supplementary Figure 8). There are two modes (mode-1 and mode-2) in hybrid 2D–3D μ-cavity, the mode-1 is confined in the WGM μ-cavity, which leading to lasing at mode-1. The coupled efficiency is altered between the gain μ-cavity and the loss μ-cavity, which altered WGM resonant wavelength from mode-1 to mode-2, leading to laser output at mode-2.

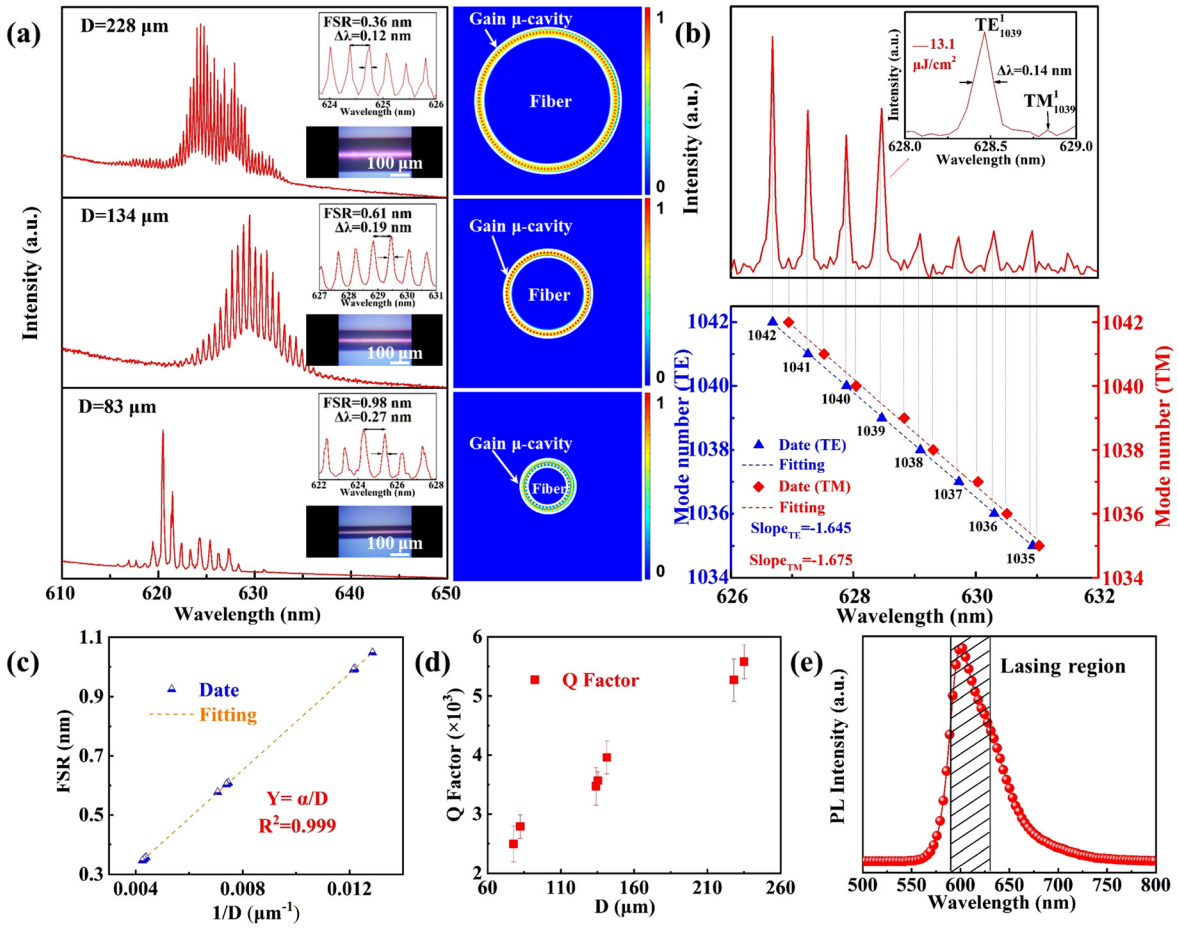

Figure 3: The relationship between lasing spectrum and diameters.
(a) WGM modulation in three fibers with different diameters above the threshold. Scale bars is 100 μm. (b) The lasing spectra is from Eq. (1). Top right illustration is the lasing peak belong to first order TE and TM, and the corresponding mode count from 1035 to 1042. (c) The relationship between FSR and the diameter of isolated polymer fiber *D*, the dashed line is fitted with Eq. (2), α is constant. (d) The relationship between *Q* factor and various diameter *D*. (e) The spontaneous emission and the highlighted area indicates lasing region.

In the experiment, there are two pump point A and B as shown in Figure 4d. The single mode (λ_A = 626.15 nm) is obtained when pumped by point-A, the single mode (λ_B = 626.80 nm) is achieved when pumped by point-B. The single mode (λ_A = 626.15 nm) is obtained when pumped point is from point-A to point-B. Furthermore, this results indicate the wavelength switch of single mode lasing can be realized by pump-control. This may demonstrate a novel way to acquire tunable single mode lasing.

Noteworthy, according to the filtering effect, the polymer fiber therein serves as an excellent gain cavity to provide multiple lasing modes while the PSP acts as a loss channel to suppress most of the lasing modes in 2D–3D hybrid μ-cavity. We can obtain the single mode lasing when the pump energy density exceeds the first threshold (61.2 μJ/cm^2). The 2D–3D hybrid μ-cavity enable single mode lasing when all but one of the lasing modes are suppressed duo to the loss μ-cavity of the PSP, and the pump density do not exceed the second threshold (101.2 μJ/cm^2) (Supplementary Figures 5 and 9). However, the multiple lasing modes will be output when the pump density exceeds the second threshold (101.2 μJ/cm^2). The number ① indicates the operating range of spontaneous emission, ② indicates the operating range of single mode lasing, and ③ indicates the operating range of multiple lasing modes in the 2D–3D hybrid μ-cavity (in Figure 4c). This work, not only study the mechanism of single mode operation, but also provides the multiple lasing modes operating range in the 2D–3D hybrid μ-cavity.

The excellent temperature responsiveness provides a feasible method to control the peak wavelength for the polymer fiber.

The thermal-induced resonant wavelength shift can be expressed as follows [43–46]:

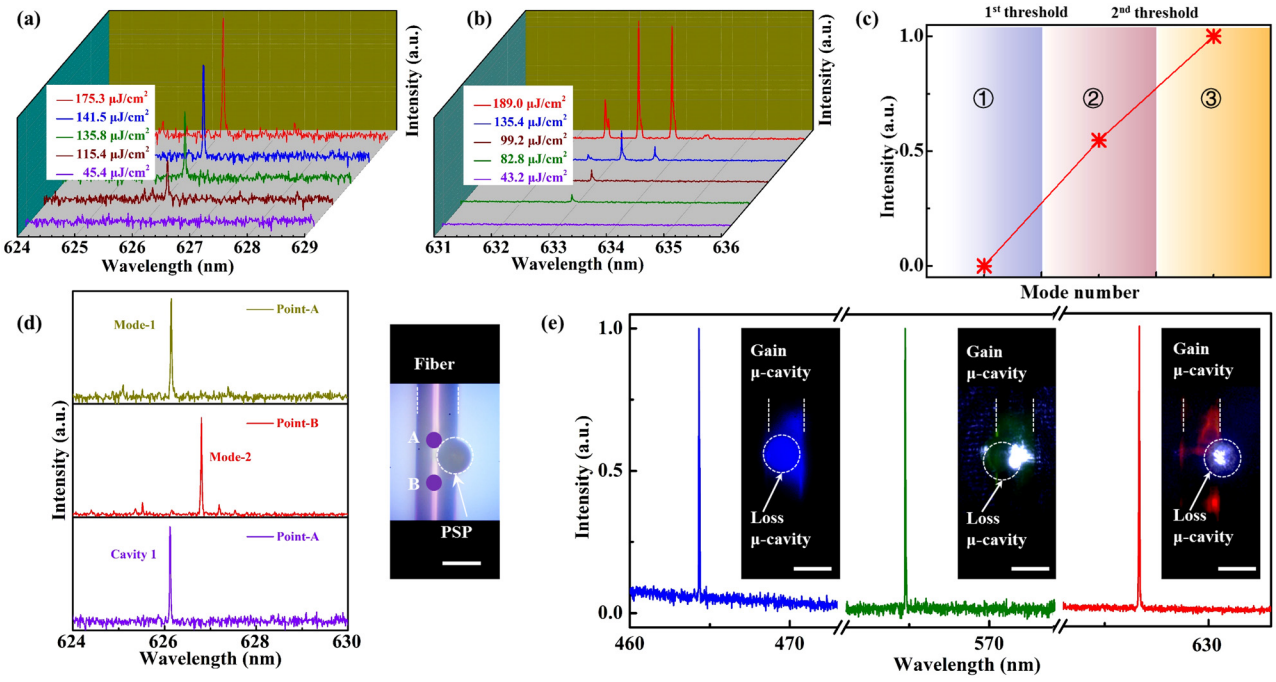

Figure 4: The optical characterization of polymer fiber and microspheres in a coupled μ-cavity.
(a) The evolution of single mode lasing in the coupled μ-cavity. (b) PL spectrum collected from the coupled μ-cavity with different pump fluence. (c) The relationship between mode number and output intensity. These areas represent no lasing, single mode lasing and multi-mode lasing from left to right in the coupled μ-cavity, respectively. The first threshold and second threshold show the threshold of single mode lasing and multi-mode lasing, respectively. The number ① indicates the range of spontaneous emission, ② indicates the operating range of single mode lasing, and ③ indicates the operating range of multimode lasing in the coupled μ-cavity, respectively. (d) The wavelength switch of single mode lasing can be realized by pump-controlled. (e) The normalized RGB single mode lasing and corresponding PL images. From left to right: the blue, green and red emissive. Scale bars are 100 μm.

$$d\lambda = \lambda\left(\frac{1}{n_{\text{eff}}}\frac{dn_{\text{eff}}}{dT} + \frac{1}{D}\frac{dD}{dT}\right)dT \tag{3}$$

The effective refractive index of gain materials (RhB) decreases with increasing the temperature [47], the peak wavelength is also blue-shifting due to preserving the conditions for WGM resonance. Derivation of formulas from Eq. (2)

$$\text{dFSR} = \frac{\lambda^2}{\pi n^2 D}dn \tag{4}$$

According to Eqs. (2) and (4)

$$\text{dFSR} = \frac{\lambda^2}{\pi n^2 D}dn = \frac{\lambda^2}{\pi n D}\frac{dn}{n} = \text{FSR}\frac{dn}{n} \tag{5}$$

$dn/n \ll 1$, so we can know the dFSR $\ll$ FSR in Eq. (5), therefore, the dispersion effect of the material have little effect on the spectral FSR. We can ignore the influence of the refractive index changes of the microsphere to the red shift of the laser modes after adding the microsphere on the fiber in the experiment.

During the measurement, Figure 5a provides the schematic diagram of the temperature sensing experimental setup. The effective refractive index of gain material (RhB) decreases with increasing the temperature [47], the peak wavelength is also blue-shifting due to preserving the conditions for WGM resonance. The blue color laser and green color laser have the same temperature responsiveness, which is the effective refractive index of gain material decreases with increasing the temperature (Supplementary Figure 14). The peak wavelength is also blue-shifting. To investigate the effect of the peak wavelength shift due to the temperature. We have observed that the evolution of PL spectrum of the polymer fiber μ-cavity is blue-shifting with increasing temperature range from 24.9 °C to 32.8 °C, and the pump power density is about 33.4 μJ/cm^2 (in Figure 5b). The PVA hydrogel will be melted under higher temperature. In a relatively closed space, the temperature range is stable. Therefore,

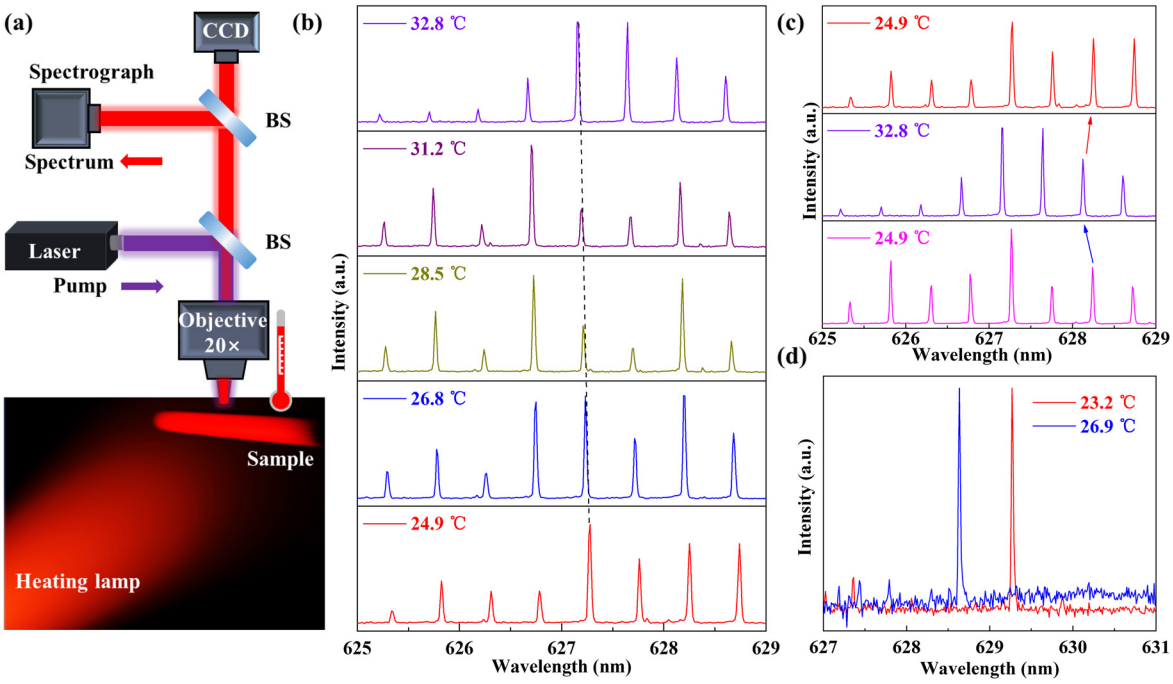

Figure 5: Tunability of the WGM peak wavelength for temperature sensing.
(a) Schematic diagram of the temperature sensing experimental setup. Inset: schematic diagram wavelength tuning achieved by controlling the environment temperature (°C). BS: beam splitter. (b) The evolution of PL spectrum is blue-shifting with increasing temperature. (c) The temperature sensor is reversible. (d) The single-mode is blue-shifting with increasing the environment temperature ranging from 23.2 °C to 26.9 °C in hybrid 2D–3D μ-cavity.

the temperatures on the polymer fiber is approximate the same as the values shown on the thermometer.

Moreover, the peak wavelength is hardly changed with increasing the pump power density from 20.71 μJ/cm^2 to 86.30 μJ/cm^2, indicating that the pump power exhibits negligible influence on peak wavelength shift at less than 86.30 μJ/cm^2 (Supplementary Figures 10 and 11). Figure 5c shows the temperature sensor is reversible (Supplementary Figure 13). The single-mode lasing is blue-shifting with increasing the environmental temperature ranging from 23.2 °Cto 26.9 °C in hybrid 2D–3D μ-cavity as shown in Figure 5d. The wavelength of the laser can return to the original position with the decreasing of temperature to the room temperature. The result indicates that the temperature sensor response is reversible. The diameter of the PSP can affect the wavelength of the selected mode (Supplementary Figure 15). Therefore, we can control the wavelength shift by precisely adjusting the temperature, which might help to achieve the expected lasing mode (Supplementary Figures 12 and 16).

The limit of detection (LOD) for temperature sensing was calculated from LOD = $3.3\sigma_D/b$ [48, 49], where b is the slope of the FWHM value versus the temperature curve and σ_D is the standard FWHM deviation. The peak wavelength drift fluctuation of 0.004 nm standard deviation. Thus, the calculated LOD of the temperature sensing is 0.36 °C.

4 Conclusions

In summary, we demonstrate a simple and general approach to realizing tunable RGB single mode lasers in the 2D–3D hybrid μ-cavity with a low threshold. Here, the polymer fiber serves as an excellent gain cavity to provide multiple lasing modes while the PSP acts as a loss channel to suppress most of the lasing modes. The colors of the RGB single mode lasers can be designed easily by changing the gain materials. Furthermore, the wavelength switch of single mode laser can be realized by pumping-controlled. The temperature responsiveness can also switch the lasing mode in the hybrid 2D–3D μ-cavity. We believe that it may provide a novel way to acquire tunable single mode lasing. Our work will provide a platform for the rational design of nanophotonic devices and on-chip communication.

Acknowledgments: The authors would like to acknowledge the National Natural Science Foundation of China (NSFC) (61822501) and the Beijing Natural Science Foundation (Z180015) for financial support.

Author contribution: Conceptualization, Tianrui Zhai; investigation, Dan Guo and Kun Ge; methodology, Zhiyang Xu; project administration, Ben Niu; resources, Jun Ruan; writing, Kun Ge. All authors have read and agreed to the published version of the manuscript.

Research funding: None declared.

Conflict of interest statement: The authors declare no conflict of interest.

References

[1] K. Heylman, N. Thakkar, E. Horak, et al., "Optical microresonators as single-particle absorption spectrometers," *Nat. Photonics*, vol. 10, pp. 788–795, 2016.

[2] B. Shen, X. Yu, Y. Zhi, et al., "Detection of single nanoparticles using the dissipative interaction in a high-Q μ-cavity," *Phys. Rev. Appl.*, vol. 5, p. 024011, 2016.

[3] M. Baaske, M. Foreman, and F. Vollmer, "Single-molecule nucleic acid interactions monitored on a label-free μ-cavity biosensor platform," *Nat. Nanotechnol*, vol. 9, p. 933, 2014.

[4] W. Chen, S. Ozdemir, G. Zhao, J. Wiersig, and L. Yang, "Exceptional points enhance sensing in an optical μ-cavity," *Nature*, vol. 548, pp. 192–196, 2017.

[5] J. Zhang, B. Peng, S. Ozdemir, et al., "A phonon laser operating at an exceptional point," *Nat. Photonics*, vol. 12, pp. 479–484, 2018.

[6] Y. Wang, S. Zeng, G. Humbert, and H. Ho, "Microfluidic whispering gallery mode optical sensors for biological applications," *Laser Photon. Rev.*, vol. 14, p. 2000135, 2020.

[7] T. Squires, R. Messinger, and S. Manalis, "Making it stick: convection, reaction and diffusion in surface-based biosensors," *Nat. Biotechnol.*, vol. 26, pp. 417–426, 2008.

[8] F. Vollmer and S. Arnold, "Whispering-gallery-mode biosensing: label-free detection down to single molecules," *Nat. Methods*, vol. 5, pp. 591–596, 2008.

[9] A. Qavi, T. Mysz, and R. Bailey, "Isothermal discrimination of single-nucleotide polymorphisms via real-time kinetic desorption and label-free detection of DNA using silicon photonic microring resonator arrays," *Anal. Chem.*, vol. 83, pp. 6827–6833, 2011.

[10] L. Pasquardini, S. Berneschi, A. Barucci, et al., "Whispering gallery mode aptasensors for detection of blood proteins," *J. Biophot.*, vol. 6, pp. 178–187, 2013.

[11] Y. Yang, S. Saurabh, J. Ward, and S. Chormaic, "High-Q, ultrathin-walled microbubble resonator for aerostatic pressure sensing," *Opt. Express*, vol. 24, pp. 294–299, 2016.

[12] Q. Lu, J. Liao, S. Liu, X. Wu, L. Liu, and L. Xu, "Precise measurement of micro bubble resonator thickness by internal aerostatic pressure sensing," *Opt. Express*, vol. 24, pp. 20855–20861, 2016.

[13] G. Haider, H. Lin, K. Yadav, et al., "A highly-efficient single segment white random laser," *ACS Nano*, vol. 12, pp. 11847–11859, 2018.

[14] T. Zhai, L. Niu, F. Cao, et al., "A RGB random laser on an optical fiber facet," *RSC Adv.*, vol. 7, pp. 45852–45855, 2017.

[15] T. Zhai, Z. Xu, S. Li, and X. Zhang, "Red-green-blue plasmonic random laser," *Opt. Express*, vol. 25, pp. 2100–2106, 2017.

[16] J. Zhao, Y. Yan, Z. Gao, et al., "Full-color laser displays based on organic printed microlaser arrays," *Nat. Commun.*, vol. 10, p. 870, 2019.

[17] Y. Yin, Z. Hu, M. Ali, et al., "Full-color micro-LED display with CsPbBr3 perovskite and CdSe quantum dots as color conversion layers," *Adv. Mater. Technol.*, vol. 5, p. 2000251, 2020.

[18] Y. Lv, Y. Li, J. Li, Y. Yan, J. Yao, and Y. Zhao, "All-color subwavelength output of organic flexible microlasers," *J. Am. Chem. Soc.*, vol. 139, pp. 11329–11332, 2017.

[19] R. Chen, V. Ta, and H. Sun, "Single mode lasing from hybrid hemispherical microresonators," *Sci. Rep.*, vol. 2, p. 244, 2012.

[20] A. Zhizhchenko, S. Syubaev, A. Berestennikov, et al., "Single-mode lasing from imprinted halide-perovskite microdisks," *ACS Nano*, vol. 13, pp. 4140–4147, 2019.

[21] X. Wang, R. Wang, J. Chen, et al., "Dynamical tuning for single mode whispering gallery mode μ-cavity lasing," *Opt. Commun.*, vol. 485, p. 126688, 2021.

[22] A. Hayat, J. Tong, C. Chen, et al., "Multi-wavelength colloidal quantum dots lasers in distributed feedback cavities," *Sci. China Inf. Sci.*, vol. 63, p. 182401, 2020.

[23] S. Dhoore, A. Köninger, R. Meyer, G. Roelkens, and G. Morthier, "Electronically tunable distributed feedback (DFB) laser on silicon," *Laser Photon. Rev.*, vol. 13, p. 1800287, 2019.

[24] Y. Fu and T. Zhai, "Distributed feedback organic lasing in photonic crystals," *Front. Optoelectron. China*, vol. 13, pp. 18–34, 2020.

[25] H. Wang, S. Liu, L. Chen, De. Shen, and X. Wu, "Dual-wavelength single-frequency laser emission in asymmetric coupled microdisks," *Sci. Rep.*, vol. 6, p. 38053, 2016.

[26] Y. Wang, C. Xu, M. Jiang, et al., "Lasing mode regulation and single-mode realization in ZnO whispering gallery microcavities by the Vernier effect," *Nanoscale*, vol. 8, p. 16631, 2016.

[27] V. Ta, R. Chen, and H. Sun, "Coupled polymer microfiber lasers for single mode operation and enhanced refractive index sensing," *Adv. Opt. Mater.*, vol. 2, pp. 220–225, 2014.

[28] L. Feng, Z. Wong, R. Ma, Y. Wang, and X. Zhang, "Single-mode laser by parity-time symmetry breaking," *Science*, vol. 346, pp. 972–975, 2014.

[29] W. Liu, M. Li, R. Guzzon, et al., "An integrated parity-time symmetric wavelength-tunable single-mode microring laser," *Nat. Commun.*, vol. 8, p. 15389, 2017.

[30] H. Hodaei, M. Miri, M. Heinrich, D. Christodoulides, and M. Khajavikhan, "Parity-time symmetric microring lasers," *Science*, vol. 346, pp. 975–978, 2014.

[31] H. Zhou, G. Feng, K. Yao, C. Yang, J. Yi, and S. Zhou, "Fiber-based tunable microcavity fluidic dye laser," *Opt. Lett.*, vol. 38, pp. 3604–3607, 2013.

[32] A. Muller, E. Flagg, M. Metcalfe, J. Lawall, and G. Solomon, "Coupling an epitaxial quantum dot to a fiber-based external-mirror microcavity," *Appl. Phys. Lett.*, vol. 95, p. 173101, 2009.

[33] H. Sun1, H. Zhang, G. Feng, H. Zhou, and S. Zhou, "Freestanding polymeric microdisk laser based on a microfiber knot," *Laser Phys. Lett.*, vol. 14, p. 055806, 2017.
[34] J. Ward and O. Benson, "WGM microresonators: sensing, lasing and fundamental optics with microspheres," *Laser Photon. Rev.*, vol. 5, pp. 553–570, 2011.
[35] X. Jiang, C. Zou, L. Wang, Q. Gong, and Y. Xiao, "Whispering-gallery microcavities with unidirectional laser emission," *Laser Photon. Rev.*, vol. 10, pp. 40–61, 2016.
[36] S. V. Frolov and Z. V. Vardeny, "Plastic microring lasers on fibers and wires," *Appl. Phys. Lett.*, vol. 72, pp. 1802–1804, 1998.
[37] S. V. Frolov, M. Shkunov, and Z. V. Vardeny, "Ring microlasers from conducting polymers," *Phys. Rev. B*, vol. 56, pp. R4363–R4366, 1997.
[38] H. Baek, J. K. Hyun, K. Chung, H. Oh, and G. Yi, "Selective excitation of Fabry-Perot or whispering-gallery mode-type lasing in GaN microrods," *Appl. Phys. Lett.*, vol. 105, p. 1699, 2014.
[39] Y. Zhao, J. Xu, A. Peng, et al., "Optical waveguide based on crystalline organic microtubes and microrods," *Angew. Chem.*, vol. 47, pp. 7301–7305, 2010.
[40] L. Zhao, Q. Shang, Y. Gao, et al., "High-temperature continuous-wave pumped lasing from large-area monolayer semiconductors grown by chemical vapor deposition," *ACS Nano*, vol. 12, pp. 9390–9396, 2018.
[41] J. Liao and L. Yang, "Optical whispering-gallery mode barcodes for high-precision and wide-range temperature measurements," *Light: Sci. Appl.*, vol. 10, p. 32, 2021.
[42] Y. Huang, Y. Chi, M. Chen, D. Tsai, D. Huang, and G. Lin, "Red/green/blue LD mixed white-light communication at 6500K with divergent diffuser optimization," *Opt. Express*, vol. 26, pp. 23397–23410, 2018.
[43] B. Li, Q. Wang, Y. Xiao, et al., "On chip, high-sensitivity thermal sensor based on high-Q polydimethylsiloxane-coated microresonator," *Appl. Phys. Lett.*, vol. 96, p. 251109, 2010.
[44] L. Yu, Y. Yin, Y. Shi, D. Dai, and S. He, "Thermally tunable silicon photonic microdisk resonator with transparent graphene nanoheaters," *Optica*, vol. 3, p. 159, 2016.
[45] L. Wan, H. Chandrahalim, C. Chen, et al., "On-chip, high-sensitivity temperature sensors based on dye-doped solid-state polymer microring lasers," *Appl. Phys. Lett.*, vol. 111, p. 061109, 2017.
[46] L. Zhao, Y. Wang, Y. Yuan, et al., "Whispering gallery mode laser based on cholesteric liquid crystal microdroplets as temperature sensor," *Opt. Commun.*, vol. 402, pp. 181–185, 2017.
[47] N. Zhang, Z. Gu, K. Wang, et al., "Quasiparity-time symmetric microdisk laser," *Laser Photon. Rev.*, vol. 11, p. 1700052, 2017.
[48] Z. Xu, T. Zhai, X. Shi, J. Tong, X. Wang, and J. Deng, "Multifunctional sensing based on an ultrathin transferrable microring laser," *ACS Appl. Mater. Interfaces*, vol. 13, pp. 19324–19331, 2021.
[49] E. Desimoni and B. Brunetti, "About estimating the limit of detection by the signal to noise approach," *Pharm. Anal. Acta*, vol. 6, p. 1000355, 2015.

Supplementary Material: The online version of this article offers supplementary material (https://doi.org/10.1515/nanoph-2021-0462).